sustainability

MDPI

Article

Long-Term Freezing Temperatures Frequency Change Effect on Wind Energy Gain (Eurasia and North America, 1950–2019)

Maddi Aizpurua-Etxezarreta [1], Sheila Carreno-Madinabeitia [2,*], Alain Ulazia [1], Jon Sáenz [3,4] and Aitor Saenz-Aguirre [1]

[1] Energy Engineering Department, University of the Basque Country (UPV/EHU), E-20600 Eibar, Spain; maizpurua018@ikasle.ehu.eus (M.A.-E.); alain.ulazia@ehu.eus (A.U.); aitor.saenz@ehu.eus (A.S.-A.)
[2] Department of Mathematics, University of the Basque Country (UPV/EHU), E-01006 Vitoria-Gasteiz, Spain
[3] Department of Physics, University of the Basque Country (UPV/EHU), E-48080 Leioa, Spain; jon.saenz@ehu.eus
[4] Plentziako Itsas Estazioa (BEGIK), University of Basque Country (UPV/EHU), E-48620 Plentzia, Spain
* Correspondence: sheila.carreno@ehu.eus

Abstract: The persistent freezing conditions in cold regions are the cause of ice accretion on mechanical and instrumental elements of wind turbines. Consequently, remarkable Annual Energy Production (AEP) losses are prone to occur in those wind farms. Following global expansion of wind energy, these areas have had increased study interest in recent years. The goal of these studies is an improved characterisation of the site for the installation of turbines, which could prevent unexpected high AEP losses due to ice accretion on them. In this context, this paper provides an estimation of the freezing temperatures frequency (FTF) at 100 m over latitudes and evaluates the changes during the last 70 years. To that end, hourly surface temperature data (2 m above surface) from the ERA5 reanalysis is used in the [50° N, 75° N] latitudinal belt for the period 1950–2019. The obtained results show an average reduction of FTF hours of 72.5 h/decade for all the domain, reaching a maximum decrease of 621 h/decade on the southeast coast of Greenland and a 60% annual reduction at a specific location in Scandinavia. In terms of AEP a maximum gain of more than 26% would be projected, as categorised by the the International Energy Agency.

Keywords: wind energy potential; global warming; ice accretion; annual energy production; ERA5; temperature; applied mathematics

Citation: Aizpurua-Etxezarreta, M.; Carreno-Madinabeitia, S.; Ulazia, A.; Sáenz, J.; Saenz-Aguirre, A. Long-Term Freezing Temperatures Frequency Change Effect on Wind Energy Gain (Eurasia and North America, 1950–2019). *Sustainability* **2022**, *14*, 5630. https://doi.org/10.3390/su14095630

Academic Editor: Domenico Curto

Received: 5 April 2022
Accepted: 1 May 2022
Published: 7 May 2022

1. Introduction

Wind energy is one of the fastest-growing global renewable electricity generation technologies. An increasing number of wind farms are erected, breaking records in new wind power installations since 2015. Global installed wind power capacity reached 744 GW in 2020, which is capable of generating 7% of the world's electricity demand, according to data provided by the World Wind Energy Association [1]. Many of the favourable areas for wind farm construction are in cold regions of high latitudes, such as Eastern and Northern Europe, North America, and Asia [2]. According to statistics from the International Energy Agency (IEA), by the end of 2015, approximately 30% of all wind turbine installations were located in cold regions [3].

These areas present great potential for wind energy exploitation for several reasons. On the one hand, from the point of view of global atmospheric circulation, polar areas are characterised by high pressure due to surface cooling; as a result of the subsidence in them, polar regions tend to be quite stable. However, in regions closer to the Equator that are thereby affected by the Ferrel cell (around 60° N in our case), there exist many low-pressure areas due to baroclinic instability. These extratropical cyclones produce wind regimes of remarkable value for the exploitation of wind energy (e.g., the Baltic Sea and the UK). It is in these latitudes where the synoptic surface westerly regime manifests itself with maximal

intensity in accordance with general atmospheric circulation patterns [4]. On the other hand, in cold climate areas, wind energy potential is 10% higher than that in other regions due to increased air density at low temperatures within seasonal changes, mainly from summer to winter [5–9]. Numerous locations in cold climate areas, such as the Swiss Alps, the northern Scandinavian coastline, many parts of China, northern USA, and Canada offer high wind-energy potential, especially during the winter months [10].

However, more than 50% of wind turbines located in cold regions are affected by various icing events in winter [11]. Temperatures below the freezing point of water and wet environments potentially lead to ice formation and icing persistence on structures exposed to wind, resulting in considerable power losses. Processes of ice formation, type, duration, and severity depend on a subset of conditions [2]. Temperature, wind speed, liquid water content, and droplet size distribution are the most important meteorological conditions to consider when studying ice formation. Nevertheless, there is a substantial lack of information, especially on the latter two variables, which can be used to assess and predict the severity and frequency of the phenomenon [12]. In addition, identical weather conditions do not always cause the same icing effects on the same turbine or even different turbines. At different operating speeds, depending on the rotor, angle of attack, rotational speed, and other factors, icing effects are different [2].

This is why it is so complex to carry out a detailed study on ice formation and production losses. Even so, several studies investigated the ice accretion process [12–17] on wind turbine blades, and its detrimental effect on the performance and power production of wind turbines [2,10,18,19]. Mapping all potential risks and site-assessment studies are keys to success in a wind farm investment [20]. The main drawback associated with ice accretion on wind turbines from which wind turbine manufacturers suffer is the considerable Annual Energy Production (AEP) loss experienced by wind turbines located in cold climate areas. The two reasons behind these losses are the reduced aerodynamic performance of iced wind-turbine blades and the unexpected stoppage periods of wind turbines due to high aerodynamic degradation.

However, according to the Intergovernmental Panel on Climate Change (IPCC) reports, annual warming [21] in the northern hemisphere is expected with global warming. Every decade since 1880, the temperature of Earth has warmed by 0.14 °C [22]. Moreover, as shown in Collins et al. [23], the number of frost days (number of days below 0 °C) is significantly reduced globally. According to Yan et al. [24], frost days, cold days, and cold nights are showing a decreasing trend in China. This suggests that temperatures below the freezing point of water for atmospheric ice formation will occur less frequently in the coming years.

In this context, the estimation of AEP losses before the installation of wind turbines is necessary for wind turbine manufacturers, especially in cold climate areas. The most suitable location for the installation of wind turbines can be selected on the basis of AEP estimations, and posterior unexpected losses that might compromise the contracts can be minimised. Our analysis examines the temporal evolution of freezing temperatures as a necessary condition for the formation of meteorological ice, and subsequent AEP losses from 1950 to 2019 to identify clear patterns in its evolution. As a result, a foundation for the site assessment, operation, and maintenance of wind turbines in northern latitudes was developed on the basis of their expected AEP losses due to icing.

The paper is organised as follows: Section 2 presents datasets and the method used in this study. Section 3 describes the results, Section 4 discusses the results, and Section 5 concludes this study.

2. Data and Methodology

2.1. Data

In this study, temperatures estimated by ERA5 [25] reanalysis at 2 m over the surface in high latitudes of the northern hemisphere were used. ERA5 is the most recent reanalysis [26] developed at the European Centre for Medium-Range Weather Forecasts

(ECMWF) and it is freely available through the Copernicus Climate Data Store. It is the fifth-generation reanalysis by the ECMWF. The available ERA5 data period was from 1950 to the present; this reanalysis archives data at an hourly output resolution and a recommended $0.25^\circ \times 0.25^\circ$ spatial resolution. Different researchers successfully validated ERA5 in wind potential assessments for both wind speed and density, and consequently temperature, even suggesting that it can lead to wind energy models [7,27,28].

According to ERA5 data observation documentation [29], temperature data from buoys are not assimilated. For this reason, in this study, two buoys were validated. One corresponded to Station 44078, OOI Irminger Sea Surface Mooring managed by the National Oceanic and Atmospheric Administration (NOAA) in Greenland (68.47° N, 9.26° W), which was used to perform validation during the period of 10 September 2014–31 December 2019. The second buoy is located on the Iceland coast (59.95° N, 39.57° W) and is available from the Pangaea Project (PANG) [30]. These data were used for validation during the period of 23 November 2007–21 August 2009. Validation was carried out by means of a Taylor diagram [31] because it shows the correlation, centred root mean standard error, and standard deviation (represented by the horizontal axis, radial distance, and horizontal axis, respectively) in the same plot. The Taylor diagram is a successful tool for the evaluation of model simulations against observed data. It is possible to visually compare three different quality indicators simultaneously. ERA5 reanalysis data are represented by a grey point in the x axis in the diagram (see Figure 1), and visual inspection allows for easily determining how close the model data (green dots) were to the buoy data (i.e., present lower error). It also randomly created 1000 new series using the bootstrap technique to ascertain the sensitivity of the point position in the Taylor diagram to the available sample.

2.2. Annual Freezing Frequency Temperature at 100 m

In order to obtain preliminary information on the presence of favourable conditions for icing in wind energy zones, a new variable was defined, namely, annual freezing temperature frequency (FTF), for which the annual hours of temperatures below 0 °C at each grid point at the hub height of the turbines were counted.

Furthermore, before obtaining the annual FTF, it is necessary to calculate temperature at hub height, which was 100 m here. According to the American Meteorological Society's Glossary of Meteorology [32], temperature inversion corresponds to a layer of the atmosphere at which temperature increases with height. This is not consistent with the most frequent behaviour, which is represented by a reduction in temperature with height. Although temperature inversions are typical at high latitudes due to surface cooling processes, this study approximated a standard atmosphere for the whole domain where temperature decreased through a constant vertical temperature gradient (Γ) in K/m (Equations (1) and (2)).

$$\Gamma = -0.0065 \text{ K m}^{-1} \quad (1)$$

$$t_{100\text{m}} = t_{2\text{m}} + \Gamma(100 \text{ m} - 2 \text{ m}) \quad (2)$$

2.3. Annual FTF Mean Data and Decadal Trends

With the annual FTF data described in the previous section, the mean annual value at each grid point was calculated for the period of 1950–2019, and results are shown in Section 3.2 as a percentage of annual hours.

In order to obtain a general decadal trend for the whole domain, annual FTF results were grouped for each decade, and linear regression was calculated with the median of each decade. Lastly, in order to analyse the temporal evolution of this variable in more detail, linear regression with annual data was calculated at each grid point. The objective was to identify areas with the steepest slope where the most important changes occurred. For this purpose, the Theil–Sen estimator was used [33,34], which robustly fits simple linear regression by choosing the median of slopes of all lines crossing each pair of points [35]. Coefficients of linear regressions were calculated, obtaining the 95% confidence interval.

In this work, the *mblm()* function of the R-cran [36] library of the same name was used. This function from the *mblm* package [37] is used to fit linear models on the basis of the Theil–Sen method.

2.4. AEP Loss Approximation

The calculation of the AEP losses of a wind turbine is based on the methodology proposed by the IEA (see Table 1). This table relates the duration of meteorological icing events with an ice class and associated potential AEP losses on the basis of expected aerodynamic performance reduction and stoppage periods due to the ice accretion that the meteorological icing would cause. Ice classes are based on measurements, and an estimate of possible best and worst cases under given icing conditions [38].

Table 1. Ice classification according to IEA.

IEA Ice Class [−]	Meteorological Icing % of Year	AEP Loss Due to Icing %
1	0–0.5	0–0.5
2	0.5–3	0.5–5
3	3–5	3–12
4	5–10	10–25
5	>10	>20

This IEA ice classification provides a first idea of the transcendence of freezing and its consequences on the AEP for a given location. This ice classification refers to long-term conditions; for individual years or winters, results may lie outside these classes. If the initial categorisation of ice is the second or higher, the regulation recommends an ice measurement campaign and detailed study of related losses [3].

The approximation of FTF to the meteorological icing duration is appropriate given that air temperature below 0 °C is a necessary condition for icing [18,39]. Therefore, provided maps and associated trends with this variable constitute a rough estimate of potential icing conditions, and should not be used as the only indicator when it comes to studying real icing conditions for the design of wind farms in cold climates. For that case, direct measurements of icing parameters (liquid water content, medium volume droplet, and wind speed) are vital and can provide more accurate information than ice maps can.

In this paper, on the basis of annual FTF approximation data, the yearly duration of meteorological icing conditions was estimated, and ice categorisation and AEP loss associated with that meteorological icing can thereby be computed, following Table 3-1 of wind energy projects in cold climates [3].

2.5. AEP Gain

The general reduction in freezing days due to global warming produces changes in AEP during the entire period (ΔAEP) that can be quantified using values in Table 1. The values of the table were linearly interpolated to establish a continuous relationship between meteorological icing duration and AEP loss intervals, and averages over decades were then calculated. ΔAEP is AEP loss in percentage in the entire period (Equation (3)).

$$\Delta AEP = AEP_{1950-1959} - AEP_{2010-2019}, \quad (3)$$

given that it is expected that $AEP_{2010-2019} < AEP_{1950-1959}$.

3. Results

3.1. ERA5 t_{2m} Validation on Two Buoys

The nearest grid point of t_{2m} from ERA5 reanalysis and buoy data was compared through the Taylor diagram in Figure 1. The validation of the Iceland and Greenland buoys had a correlation of above 0.8 and root mean square error of less than 1 °C and

2 °C. The standard deviation of the model was very similar to the observation in Iceland, but in Greenland, ERA5 showed greater variability than that of the buoy measurements, almost doubling its standard deviation from 2 to 3.6 °C. Although worse validation data were expected nearer the Arctic (i.e., Greenland) because of the systematic error found by Wang et al. [40] at temperatures below −25 °C and the lack of data in the Artic area due to the harsh environmental conditions (see Section 4), validation was very good in both cases in terms of correlation and relative errors.

This was an expected result, given that ERA5 performs better in terms of accuracy than previous models and regarding reanalysis, such as ERA-Interim, even in the remote weather stations of the Antarctic, with fewer data assimilation sources than those in the northern hemisphere and the Arctic. ERA5 is highly accurate, and its higher spatial and temporal resolution significantly reduces cold coastal biases identified in ERA-Interim, increasing accuracy representing the wind [41].

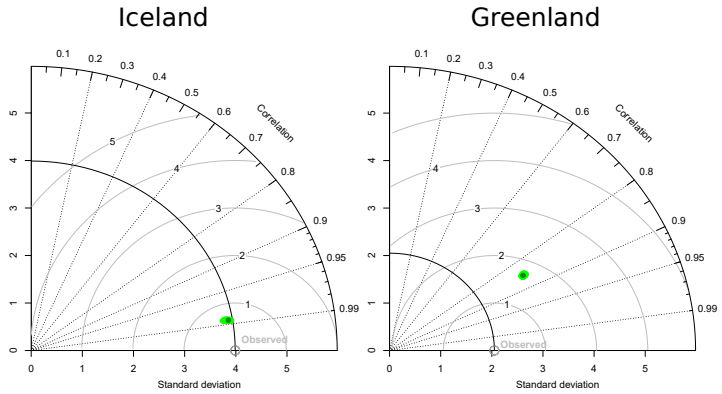

Figure 1. Taylor diagrams of t_{2m} between ERA5 and Iceland and Greenland buoys.

3.2. Annual FTF Mean Data and Decadal Trends

Annual FTF data at each grid point in high latitudes (50° N, 75° N) of the northern hemisphere during 1950–2019 were quantified, and the mean of the results is shown in Figure 2. The figure shows that freezing is higher over land than that over the sea, and increases at higher latitudes. In the Arctic Ocean, high values of annual FTF were observed. At below about 60° N latitude, annual FTF was zero in offshore areas, especially in areas affected by the transportation of energy due to the Atlantic Ocean Gulf Stream. Maximal annual FTF was found in inland areas in Greenland, where all hours of the year are below 0 °C.

In relation to decadal annual FTF changes, for a domain covering all high latitudes (50° N, 75° N), a −72.5 h/decade slope is shown in Figure 3. This slope had a large 95% confidence interval [−84.33, −50.21] h/decade. Because the study area is large, it is difficult to assign a general behaviour to it. However, lower and upper limits of the slope's confidence interval were negative, and this confirmed an overall descent in the historical evolution of annual FTF. This descent was higher in the last three decades (1990–2019). In order to identify zones with different behaviours, the slope of annual FTF at each grid point was calculated to obtain more accurate information (Figure 4).

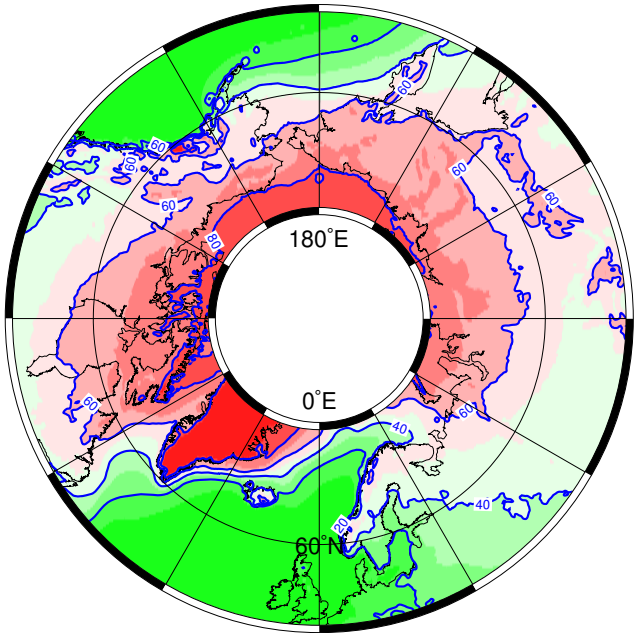

Figure 2. Mean value of annual FTF at 100 m for ERA5 in 1950–2019. Results in percentage of hours per year.

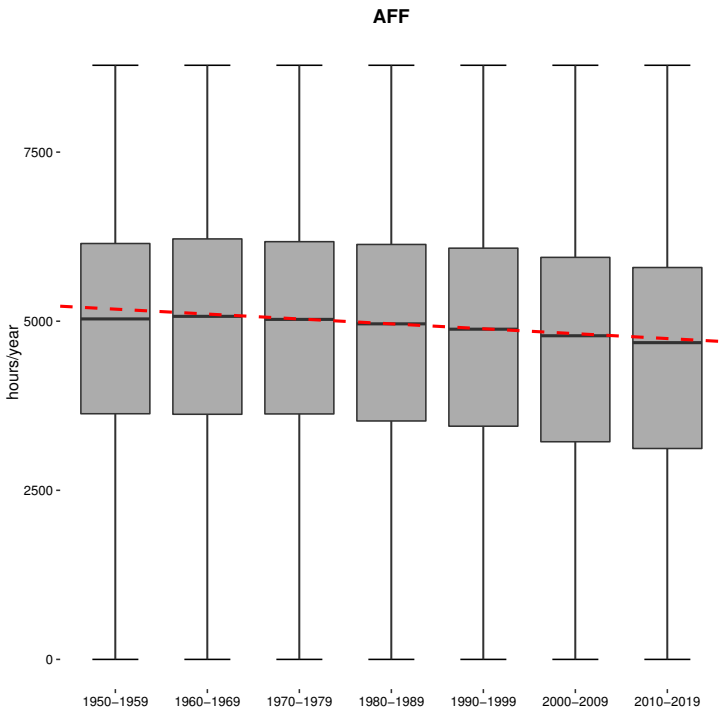

Figure 3. Decadal box plot of annual FTF in 1950–2019 from ERA5 data. Red dashed line, Theil–Sen estimator of median of annual values.

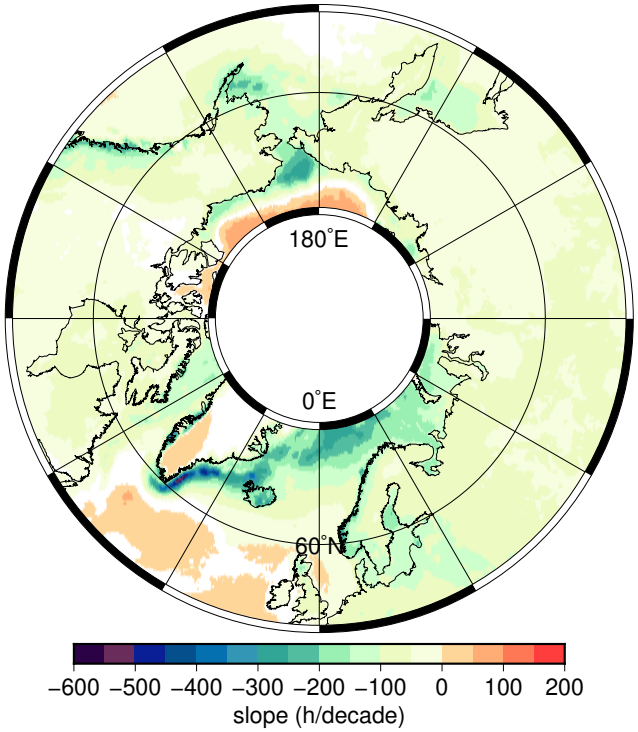

Figure 4. Map of decadal trends in annual FTF for 1950–2019. Slope obtained using Theil–Sein estimator of decadal ERA5 data. White values, nonsignificant.

Most of the results were significant at the 95% confidence level, but 7% were not significant and are plotted with white. The highest reduction up to −621 h/decade is located on the southeast coast of Greenland. Steep declines are also observed in Iceland, Norway, the Baltic Sea and west of Alaska. In offshore areas where the mean annual FTF values (Figure 2) are zero, the trend is around zero or slightly positive. However, in the offshore areas of higher latitudes, where there are high annual FTF mean values, the negative slope is very pronounced, being maximum over the sea.

Finally, increasing the detail over the Scandinavian area, location of wind farms and annual FTF information are combined. Figure 5 shows the location of wind farms registered up to 2016, with a total capacity of 515 MW. These data were extracted from the Wind Power Database [42]. The annual FTF slopes are also shown in Figure 5. In the area shown (4.5° E–40° E, 52.5° N–75° N) an average slope of −119 h/decade is obtained. The maximum slope, −310 h/decade is located in southwest coast of Norway at 5.75° E, 62° N point. The decrease in the annual FTF at this point is analysed by taking the values of the annual hours of both extremes 1950 (3623 h) and 2019 (1447 h). A reduction of 60% is obtained in a place where wind farms are already placed.

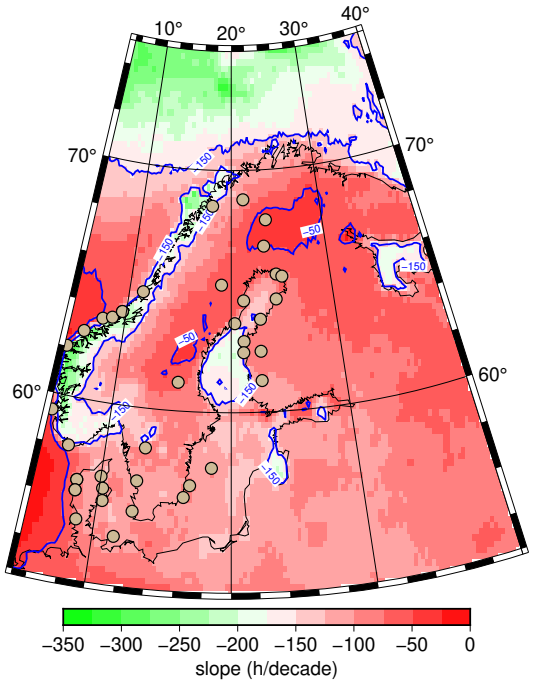

Figure 5. Map of the decadal trends in annual FTF for period 1950–2019 obtained using Theil-Sein estimator and ERA5 data in Scandinavian area. The green dots indicate the location of wind farms.

3.3. AEP Losses Approximation and Gain

The temporal evolution of the IEA ice categorisation approximation, see Table 1, for the analysed regions and during the analysed decades is presented in Figure 6. Each IEA ice category is highlighted in the maps in Figure 6 with a different color. The changes of the colors over the decades is indicative of the transformation of the freezing severity decade by decade in the region.

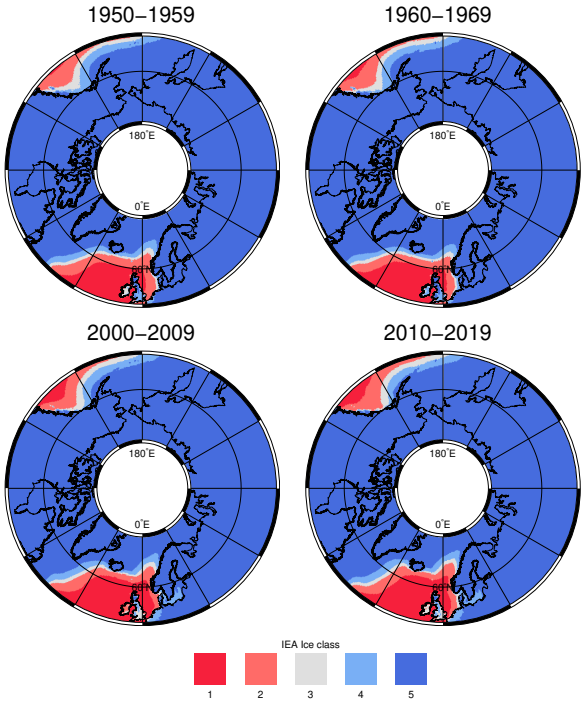

Figure 6. Decadal distribution of IEA ice class according to Table 1. Categorisation based on annual FTF approximation data at 100 m.

Analysis of the temporal evolution of the temperature over the years mainly showed that it led to mild favourable conditions, especially in the western coast of Canada, the Baltic Sea, the United Kingdom, and the Atlantic Ocean near Iceland and Norway. This reduction in turn caused a reduction in environmental harshness for the operation and maintenance of wind turbines in cold climate conditions, and improved their energy production. In the last decade (2010–2019), these conditions were weakened. In the Baltic Sea and Scotland, freezing severity decreased from Category 5 to Category 4. The Norwegian Sea is likewise one of the most affected places, together with western Canada (Figure 7). This weakening would be accompanied by a decrease in AEP losses from wind turbines, that is, an AEP gain.

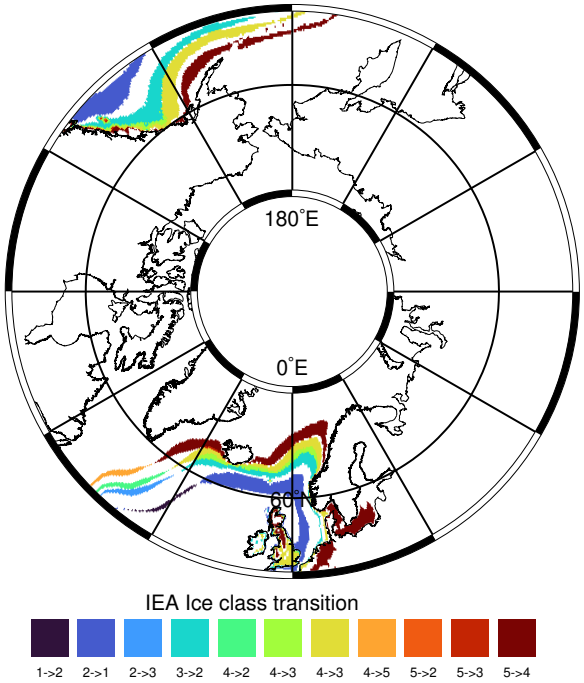

Figure 7. Transitions in IEA ice class according to Table 1 from first (1950–1959) to last decade (2010–2019). Categorisation based on annual FTF approximation data at 100 m.

The temporal evolution of ice categorisation thus shows a clear pattern of a reduction in freezing over the decades, especially in areas with a cold climate due to their prolonged exposure to icing conditions. On the basis of the long-term trend of the meteorological icing, AEP losses of a wind turbine located in a cold climate area are thus expected to decrease.

Given the results in the previous maps and the well-known wind energy potential of the locations, the Gulf of Alaska and Northern Europe were selected for deeper study.

3.3.1. AEP Gain in Gulf of Alaska

A milder climate causes fewer icing events, and its effect on wind turbine performance is lower. For instance, in the Gulf of Alaska, in domain 180° W, 120° W, 50° N, 65° N, a mean reduction in AEP losses of 5.19% was observed by comparing decades from 1950 to 2019 (Figure 8). This is a clear indicator (under currently expected climatological trends) of the favourable long-term prospective for the installation of wind turbines in cold climate areas.

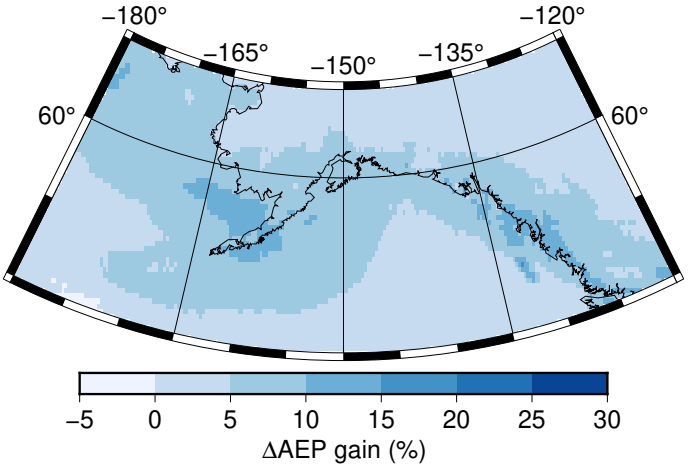

Figure 8. AEP gain in Gulf of Alaska (1950–1959 minus 2010–2019).

3.3.2. AEP Gain in Northern Europe

The same study was carried out for Northern Europe, specifically for domain 50° W, 30° E and 50° N, 75° N. The mean reduction in AEP losses of the aforementioned domain was 4.65%, calculated by comparing decades 1950 and 2019 (Figure 9). The maximal gain of 26.78% was again located on the southeast coast of Greenland (34.5° W, 65° N).

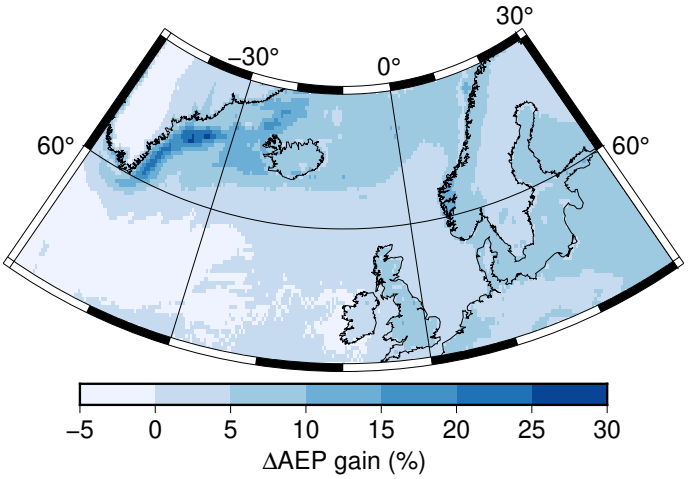

Figure 9. AEP gain in northern Europe (1950–1959 minus 2010–2019).

4. Discussion

Wind energy plays a key role in the transition to sustainable electrical energy infrastructure. Wind turbines are expected to operate in all countries over the world subject to their electrical grid restrictions and environmental characteristics. One type of the main unfavourable locations for the operation of wind turbines is cold climate sites, where wind turbines are persistently forced to deal with ice accretion of their mechanical and instrumental elements. On account of this ice accretion, the performance of the wind turbines is usually severely worsened due to reduced aerodynamic behaviour. Important and unaccounted for power production losses are prone to occur as a result. This is a major issue for wind turbine manufacturers, as great power production losses could compromise the fulfilment of signed contracts.

Moreover, while wind turbines are allowed to operate with ice on their blades in some countries, other countries forbid their operation due to the risks associated to the operation and maintenance of wind turbines with ice, especially for people in nearby areas. The potential increase in loads due to icing could lead to an increased risk of premature mechanical failure, reducing the turbine's lifetime and, in the worst cases, resulting in

the critical failure of the mast and measurement components. Other problems include the potential for increased noise emissions, and health and safety issues arising from ice throw [3]. In those cases, a wind farm located in a cold climate area could be stopped for long time periods, and AEP losses are very high. Hence, meteorological analyses for the correct site selection of wind farms taking into account the climatological frequency of icing in order to avoid previously stated problems are especially important.

In this context, global warming is causing a collateral beneficial effect for the wind energy industry. We identified a huge AEP gain (around 20%) within five decades due to the reduction in icing hours in very important locations such as Alaska. National Renewable Energies Laboratory (NREL) reports showed that Alaska has net offshore wind energy potential that is 68% higher than that of all other states combined [43,44]. Areas near Canada showed its enormous offshore wind energy potential [45]. The same can be said for our results around Northern Europe, also suggesting huge offshore wind energy potential in the North, Baltic, and Norwegian Seas [46–48] (see Figure 5). These remote areas near Arctic meteorological conditions should thus be deeply studied because they are suffering significant climatic variations.

The Arctic has endured significant changes in recent decades, with the decline in sea ice being one of the most prominent indicators of climate change [40]. However, in this paper, a positive trend of the annual FTF for the Arctic Ocean was obtained at around 75° N latitudes, a result that contrasts with reality. Due to the lack of in situ observations, this study was entirely based on data from ERA5 reanalysis, which provides high-quality results [7,27]. However, it also shows biases and uncertainties when compared to in situ observations in the Arctic, which is not relevant to the wind energy industry due to its extreme remoteness. In any case, the wide coverage of Arctic regions during winter is complicated due to the harsh environmental conditions, particularly for long-term analyses such as the one carried out in this study. Wang et al. [40] determine a mean systematic error of 5.4 °C in the daily mean t_{2m} from the surface, during winter, and especially when the temperature is below −25 °C in the Atlantic and Pacific sectors. This work was carried out at 100 m above the surface, so there was a large amount of temperature data below −25 °C, which could have lead to errors. In addition, the assumption in Section 2.2 of a standard atmosphere when raising the temperature by lapse rate to 100 meters may have conditioned the Arctic results, particularly over land. This is because, as mentioned in Section 2.2, at high latitudes, temperature inversions are typical due to surface cooling; so, in this case, a standard atmosphere would not be observed.

5. Conclusions

In this work, a first approximation of the annual FTF at 100 m in the high latitudes of the Northern Hemisphere was performed using ERA5 reanalysis temperature data from 1950 to 2019.

Very interesting results were obtained for the wind industry in the areas of, for example, Iceland, Alaska, Scandinavia and the Baltic Sea because these have high wind potential, and are highly favoured due to the melting and weakening of ice due to climate change. According to the the Wind Power Database [42], there are around 3241 wind farm projects offshore and onshore in the Baltic Sea and Scandinavia, with some of them shown in Figure 5, with an installed capacity of over 48 GW. Losses in the AEP of these farms would significantly decrease due to the reduction in FTF with consequent AEP gain, together with a reduction in losses in future wind farms of Alaska, which also shows a huge offshore wind energy potential.

The results presented in this paper, corresponding to the past seven decades, show that the analysis of future projections due to climate change can be very important for the wind industry because the expected reduction in icing hours should lead to an increase in AEP. Data in Figure 7 describe the observed transitions in ice categories, this Supplementary Material is publicly distributed as a dataset in an open repository [49] because they might be helpful for final users (e.g., governments and wind farm planners). The study of this

problem by using results from the Coupled Model Intercomparison Project (Phases 5 and 6, CMIP5 and CMIP6) runs forced by different representative concentration pathways (RCP) or shared socioeconomic pathways (SSP), the right tools to ascertain the expected reduction in icing in the next decades. Temperature is one of the most frequently analysed parameters in CMIP5 or CMIP6 runs [50,51]. During the 21st century, if greenhouse gas (GHG) emissions continue growing according to RCP4.5 (medium confidence) and RCP8.5 (high confidence), the results of CMIP6 models show that global mean surface temperature for the period of 2081–2100 is expected to rise between 2.1 and 3.5 °C (RCP4.5), and 3.3 and 5.7 °C (RCP8.5) [21], and freezing hours are directly related to temperature compared to the reference period of 1986–2005. This undoubtedly affects the amount of icing hours, which are directly related to temperature. However, previous results refer to global mean temperature anomalies, but regional differences still appear, so properly downscaled data from global runs must be used in different regions of the world.

In future studies, humidity data should be introduced in order to improve the characterisation of meteorological icing frequency. The temperature and the liquid water content of the atmosphere are the most important meteorological conditions to consider when studying ice formations. Because of this, a second approximation is needed by adding humidity data to existing temperature data in future studies. Moreover, a similar study should be developed in the southern hemisphere connecting past evolution with future projections, mainly around cold areas with relevant wind energy potential such as southern Chile [52], where the feasibility of new offshore wind energy projects is also studied [53], southern Argentina [54], or New Zealand [55].

Supplementary Materials: The following supporting information can be downloaded at: https://www.mdpi.com/article/10.3390/su14095630/s1.

Author Contributions: Conceptualisation, S.C.-M., A.U., M.A.-E., J.S. and A.S.-A.; methodology, S.C.-M., A.U. and M.A.-E.; software, S.C.-M., A.U., M.A.-E. and J.S.; validation, S.C.-M.; writing—original draft preparation, M.A.-E.; writing—review and editing, S.C.-M., A.U., J.S. and A.S.-A.; visualisation, S.C.-M., J.S. and M.A.-E.; supervision, J.S., A.U. and A.S.-A.; project administration, J.S. and A.U.; funding acquisition, J.S. and A.U. All authors have read and agreed to the published version of the manuscript.

Funding: This paper is part of the project PID2020-116153RB-I00 funded by MCIN/AEI/10.13039/501100011033, and also received funding from the University of Basque Country (UPV/EHU project GIU20/008).

Institutional Review Board Statement: Not applicable.

Informed Consent Statement: Not applicable.

Data Availability Statement: Publicly available datasets were used in this study. ERA5 [25] data were downloaded through the Copernicus Climate Change Service (C3S) Climate Data Store. Data from one of the buoys were from the National Oceanic and Atmospheric Administration, and data from the other were from the Pangaea Project (PANG) [30]. Ice class categorisation transition results from 1950–1959 to 2010–2019 in high latitudes (Figure 7) are available in the following data repository: https://doi.org/10.5281/zenodo.6502404 (accessed on 1 April 2022).

Conflicts of Interest: The authors declare no conflict of interest.

Abbreviations

The following abbreviations are used in this manuscript:

AEP	Annual Energy Production
FTF	Freezing Frequency Temperature
IEA	International Energy Agency
IPCC	Intergovernmental Panel on Climate Change
NOAA	National Oceanic and Atmospheric Administration
NREL	National Renewable Energies Laboratory
RCP	Representative Concentration Pathways
SSP	Shared Socioeconomic Pathways
GHG	Greenhouse Gas

References

1. Association, W.W.E. Worldwide Wind Capacity Reaches 744 Gigawatts—An Unprecedented 93 Gigawatts added in 2020. 2021. Available online: https://wwindea.org/worldwide-wind-capacity-reaches-744-gigawatts/ (accessed on 18 June 2021).
2. Battisti, L. *Wind Turbines in Cold Climates: Icing Impacts and Mitigation Systems*; Springer: Berlin/Heidelberg, Germany, 2015.
3. Bredesen, R.E.; Vindteknikk, K.; Jordaens, P.J.; Owi-lab, S.; Khadiri-Yazami, B.Z.; Klintström, R.; Krenn, S.A.; Verein, E.; Lehtomäki, A.V.; Ronsten, G.; et al. *Expert Group Study on Recommended Practices 13. Wind Energy Projects in Cold Climates 2. Edition*; International Energy Agency: France, Paris, 2017
4. Wallace, J.M.; Hobbs, P.V. *Atmospheric Science: An Introductory Survey*; Elsevier: Amsterdam, The Netherlands, 2006; Volume 92.
5. Lamraoui, F.; Fortin, G.; Benoit, R.; Perron, J.; Masson, C. Atmospheric icing impact on wind turbine production. *Cold Reg. Sci. Technol.* **2014**, *100*, 36–49. [CrossRef]
6. Ulazia, A.; Gonzalez-Roji, S.J.; Ibarra-Berastegi, G.; Carreno-Madinabeitia, S.; Saenz, J.; Nafarrate, A. Seasonal Air Density Variations over The East of Scotland and The Consequences for Offshore Wind Energy. In Proceedings of the 2018 7th International Conference on Renewable Energy Research and Applications (ICRERA), Paris, France, 14–17 October 2018; pp. 261–265.
7. Ulazia, A.; Sáenz, J.; Ibarra-Berastegi, G.; González-Rojí, S.J.; Carreno-Madinabeitia, S. Global estimations of wind energy potential considering seasonal air density changes. *Energy* **2019**, *187*,115938. [CrossRef]
8. Ulazia, A.; Ibarra-Berastegi, G.; Sáenz, J.; Carreno-Madinabeitia, S.; González-Rojí, S.J. Seasonal correction of offshore wind energy potential due to air density: Case of the Iberian Peninsula. *Sustainability* **2019**, *11*, 3648. [CrossRef]
9. Ulazia, A.; Nafarrate, A.; Ibarra-Berastegi, G.; Sáenz, J.; Carreno-Madinabeitia, S. The consequences of air density variations over northeastern Scotland for offshore wind energy potential. *Energies* **2019**, *12*, 2635. [CrossRef]
10. Barber, S.; Wang, Y.; Jafari, S.; Chokani, N.; Abhari, R.S. The impact of ice formation on wind turbine performance and aerodynamics. *J. Sol. Energy Eng. Trans. ASME* **2011**, *133*, 011007. [CrossRef]
11. Gao, L.; Hu, H.; Sharma, A.; Ward, T.; Hu, S.; Wang, X. Experimental Investigations on Wind Turbine Icing Physics and Anti-/de-Icing Technology. Available online: https://dr.lib.iastate.edu/entities/publication/7e1f84ec-2724-471d-88b2-89614a4d5039 (accessed on 1 April 2022).
12. Nygaard, B.E.K.; Kristjánsson, J.E.; Makkonen, L. Prediction of in-cloud icing conditions at ground level using the WRF model. *J. Appl. Meteorol. Climatol.* **2011**, *50*, 2445–2459. [CrossRef]
13. Han, Y.; Palacios, J.; Schmitz, S. Scaled ice accretion experiments on a rotating wind turbine blade. *J. Wind Eng. Ind. Aerodyn.* **2012**, *109*, 55–67. [CrossRef]
14. Villalpando, F.; Reggio, M.; Ilinca, A. Prediction of ice accretion and anti-icing heating power on wind turbine blades using standard commercial software. *Energy* **2016**, *114*, 1041–1052. [CrossRef]
15. Gao, L.; Liu, Y.; Hu, H. An experimental investigation on the dynamic glaze ice accretion process over a wind turbine airfoil surface. *Int. J. Heat Mass Transf.* **2020**, *149*. [CrossRef]
16. Li, Y.; Tagawa, K.; Feng, F.; Li, Q.; He, Q. A wind tunnel experimental study of icing on wind turbine blade airfoil. *Energy Convers. Manag.* **2014**, *85*, 591–595. [CrossRef]
17. Pena, D.; Hoarau, Y.; Laurendeau, E. A single step ice accretion model using Level-Set method. *J. Fluids Struct.* **2016**, *65*, 278–294. [CrossRef]
18. Gao, L.; Tao, T.; Liu, Y.; Hu, H. A field study of ice accretion and its effects on the power production of utility-scale wind turbines. *Renew. Energy* **2021**, *167*, 917–928. [CrossRef]
19. Gao, L.; Dasari, T.; Hong, J. Wind farm icing loss forecast pertinent to winter extremes. *Sustain. Energy Technol. Assess.* **2022**, *50*, 101872. [CrossRef]
20. Zalhaf, A.S.; Elboshy, B.; Kotb, K.M.; Han, Y.; Almaliki, A.H.; Aly, R.M.; Elkadeem, M. A High-Resolution Wind Farms Suitability Mapping Using GIS and Fuzzy AHP Approach: A National-Level Case Study in Sudan. *Sustainability* **2021**, *14*, 358. [CrossRef]
21. Zhongming, Z.; Linong, L.; Xiaona, Y.; Wangqiang, Z.; Wei, L. *AR6 Synthesis Report: Climate Change 2022*; The Intergovernmental Panel on Climate Change (IPCC): Geneva, Switzerland, 2022.
22. Lindsey, R.; Dahlman, L. Climate Change: Global Temperature. Climate. gov. Available online: https://www.climate.gov/news-features/understanding-climate/climate-change-global-temperature (accessed on 1 April 2022)

23. Collins, M.; Knutti, R.; Arblaster, J.; Dufresne, J.L.; Fichefet, T.; Friedlingstein, P.; Gao, X.; Gutowski, W.J.; Johns, T.; Krinner, G.; et al. Long-term climate change: Projections, commitments and irreversibility. In *Climate Change 2013-The Physical Science Basis: Contribution of Working Group I to the Fifth Assessment Report of the Intergovernmental Panel on Climate Change*; Cambridge University Press: Cambridge, UK 2013; pp. 1029–1136.
24. Yan, W.X.; Zhao, J.F.; Li, J.P.; Wang, Y.X. Assessment of Seasonal Variability of Extreme Temperature in Mainland China under Climate Change. *Sustainability* **2021**, *13*, 12462. [CrossRef]
25. Hersbach, H.; Bell, B.; Berrisford, P.; Hirahara, S.; Horányi, A.; Muñoz-Sabater, J.; Nicolas, J.; Peubey, C.; Radu, R.; Schepers, D.; et al. The ERA5 global reanalysis. *Q. J. R. Meteorol. Soc.* **2020**, *146*, 1999–2049. [CrossRef]
26. Hersbach, H. The ERA5 Atmospheric Reanalysis. In Proceedings of the AGU Fall Meeting Abstracts, San Francisco, CA, USA, 12–16 December 2016; Volume 2016, p. NG33D–01.
27. Olauson, J. ERA5: The new champion of wind power modelling? *Renew. Energy* **2018**, *126*, 322–331. [CrossRef]
28. Soukissian, T.H.; Karathanasi, F.E.; Zaragkas, D.K. Exploiting offshore wind and solar resources in the Mediterranean using ERA5 reanalysis data. *Energy Convers. Manag.* **2021**, *237*, 114092. [CrossRef]
29. ERA5: Data Documentation. Available online: https://confluence.ecmwf.int/display/CKB/ERA5%3A+data+documentation#ERA5:datadocumentation-Observations,year={} (accessed on 1 April 2022).
30. Petersen, G.N. Meteorological buoy measurements in the Iceland Sea, 2007–2009. *Earth Syst. Sci. Data* **2017**, *9*, 779–789. [CrossRef]
31. Taylor, K.E. Summarizing multiple aspects of model performance in a single diagram. *J. Geophys. Res. Atmos.* **2001**, *106*, 7183–7192. [CrossRef]
32. American Meteorological Society. Glossary of Meteorology. Available online: https://glossary.ametsoc.org/wiki/Welcome (accessed on 1 April 2022).
33. Theil, H. *A Rank-Invariant Method of Linear and Polynomial Regression Analysis*; Koninalijke Nederlandse Akademie van Weinenschatpen: Amsterdam, The Netherlands, 1950; pp. 386–392.
34. Sen, P.K. Estimates of the Regression Coefficient Based on Kendall's Tau. *J. Am. Stat. Assoc.* **1968**, *63*, 1379–1389. [CrossRef]
35. Tian, T.S. WILCOX, RR (2010) Fundamentals of Modern Statistical Methods: Substantially Improving Power and Accuracy. 2011. Available online: https://link.springer.com/book/10.1007/978-1-4757-3522-2 (accessed on 1 April 2022).
36. R Core Team. *R: A Language and Environment for Statistical Computing*; R Foundation for Statistical Computing: Vienna, Austria, 2021.
37. Komsta, L. CRA—Package Mblm. Available online: https://cran.r-project.org/web/packages/mblm/index.html (accessed on 1 April 2022).
38. Cattin, R. *IEA R&D Wind Task 19 «Wind Energy in Cold Climates» on Behalf of IEA RD&D Wind Task 19: «Wind Energy in Cold Climates» Validation of the IEA Task 19 Ice Classification*; International Energy Agency (IEA): Paris, France, 2016.
39. Carrière, J.M.; Alquier, S.; Le Bot, C.; Moulin, E. Statistical verification of forecast icing risk indices. *Meteorol. Appl.* **1997**, *4*, 115–130. [CrossRef]
40. Wang, C.; Graham, R.M.; Wang, K.; Gerland, S.; Granskog, M.A. Comparison of ERA5 and ERA-Interim near-surface air temperature, snowfall and precipitation over Arctic sea ice: Effects on sea ice thermodynamics and evolution. *Cryosphere* **2019**, *13*, 1661–1679. [CrossRef]
41. Tetzner, D.; Thomas, E.; Allen, C. A Validation of ERA5 Reanalysis Data in the Southern Antarctic Peninsula—Ellsworth Land Region, and Its Implications for Ice Core Studies. *Geosciences* **2019**, *9*, 289. [CrossRef]
42. Wind Energy Database. Available online: https://www.thewindpower.net/index.php (accessed on 1 April 2022).
43. Doubrawa Moreira, P.; Scott, G.N.; Musial, W.D.; Kilcher, L.F.; Draxl, C.; Lantz, E.J. *Offshore Wind Energy Resource Assessment for Alaska*; National Renewable Energy Lab.(NREL): Golden, CO, USA, 2018.
44. Musial, W.; Heimiller, D.; Beiter, P.; Scott, G.; Draxl, C. *Offshore Wind Energy Resource Assessment for the United States*; National Renewable Energy Lab. (NREL): Golden, CO, USA, 2016.
45. Dong, C.; Huang, G.G.; Cheng, G. Offshore wind can power Canada. *Energy* **2021**, *236*, 121422. 2021.121422. [CrossRef]
46. Rusu, E. An evaluation of the wind energy dynamics in the Baltic Sea, past and future projections. *Renew. Energy* **2020**, *160*, 350–362. [CrossRef]
47. Schillings, C.; Wanderer, T.; Cameron, L.; van der Wal, J.T.; Jacquemin, J.; Veum, K. A decision support system for assessing offshore wind energy potential in the North Sea. *Energy Policy* **2012**, *49*, 541–551. [CrossRef]
48. Meier, K. Hydrogen production with sea water electrolysis using Norwegian offshore wind energy potentials: Techno-economic assessment for an offshore-based hydrogen production approach with state-of-the-art technology. *Int. J. Energy Environ. Eng.* **2014**, *5*, 1–12. [CrossRef]
49. Aizpurua-Etxezarreta, M.; Carreno-Madinabeitia, S.; Ulazia, A.; Sáenz, J.; Saenz-Aguirre, A. Ice Class Categorization Transition from 1950–1959 to 2010–2019 in High Latitudes. 2022. Available online: https://zenodo.org/record/6502404#.YnLWe-hBxPY (accessed on 1 April 2022).
50. Eyring, V.; Bony, S.; Meehl, G.A.; Senior, C.A.; Stevens, B.; Stouffer, R.J.; Taylor, K.E. Overview of the Coupled Model Intercomparison Project Phase 6 (CMIP6) experimental design and organization. *Geosci. Model Dev.* **2016**, *9*, 1937–1958. [CrossRef]
51. Fan, X.; Miao, C.; Duan, Q.; Shen, C.; Wu, Y. The Performance of CMIP6 Versus CMIP5 in Simulating Temperature Extremes Over the Global Land Surface. *J. Geophys. Res. Atmos.* **2020**, *125*. [CrossRef]

52. Watts, D.; Oses, N.; Pérez, R. Assessment of wind energy potential in Chile: A project-based regional wind supply function approach. *Renew. Energy* **2016**, *96*, 738–755. [CrossRef]
53. Mattar, C.; Cabello-Españon, F.; Alonso-de Linaje, N.G. Towards a Future Scenario for Offshore Wind Energy in Chile: Breaking the Paradigm. *Sustainability* **2021**, *13*, 7013. [CrossRef]
54. Labriola, C. Wind Energy in Argentina: Actuality and Prospects. In *The Age of Wind Energy*; Springer: Berlin/Heidelberg, Germany, 2020; pp. 147–173.
55. Kelly, G. History and potential of renewable energy development in New Zealand. *Renew. Sustain. Energy Rev.* **2011**, *15*, 2501–2509. [CrossRef]